JVI Journals.ASM.org

The Multiplicity of Cellular Infection Changes Depending on the Route of Cell Infection in a Plant Virus

Serafín Gutiérrez,[a]* Elodie Pirolles,[a] Michel Yvon,[a] Volker Baecker,[b] Yannis Michalakis,[c] Stéphane Blanc[a]

INRA, UMR 385 BGPI, CIRAD-INRA-SupAgro, Montpellier, France[a]; CNRS, Montpellier RIO Imaging, CRBM, CNRS, UMR 5237, Montpellier, France[b]; CNRS, MIVEGEC, UMR CNRS-IRD-UM1-UM2 5290, Montpellier, France[c]

ABSTRACT

The multiplicity of cellular infection (MOI) is the number of virus genomes of a given virus species that infect individual cells. This parameter chiefly impacts the severity of within-host population bottlenecks as well as the intensity of genetic exchange, competition, and complementation among viral genotypes. Only a few formal estimations of the MOI currently are available, and most theoretical reports have considered this parameter as constant within the infected host. Nevertheless, the colonization of a multicellular host is a complex process during which the MOI may dramatically change in different organs and at different stages of the infection. We have used both qualitative and quantitative approaches to analyze the MOI during the colonization of turnip plants by *Turnip mosaic virus*. Remarkably, different MOIs were observed at two phases of the systemic infection of a leaf. The MOI was very low in primary infections from virus circulating within the vasculature, generally leading to primary foci founded by a single genome. Each lineage then moved from cell to cell at a very high MOI. Despite this elevated MOI during cell-to-cell progression, coinfection of cells by lineages originating in different primary foci is severely limited by the rapid onset of a mechanism inhibiting secondary infection. Thus, our results unveil an intriguing colonization pattern where individual viral genomes initiate distinct lineages within a leaf. Kin genomes then massively coinfect cells, but coinfection by two distinct lineages is strictly limited.

IMPORTANCE

The MOI is the size of the viral population colonizing cells and defines major phenomena in virus evolution, like the intensity of genetic exchange and the size of within-host population bottlenecks. However, few studies have quantified the MOI, and most consider this parameter as constant during infection. Our results reveal that the MOI can depend largely on the route of cell infection in a systemically infected leaf. The MOI is usually one genome per cell when cells are infected from virus particles moving long distances in the vasculature, whereas it is much higher during subsequent cell-to-cell movement in mesophyll. However, a fast-acting superinfection exclusion prevents cell coinfection by merging populations originating from different primary foci within a leaf. This complex colonization pattern results in a situation where within-cell interactions are occurring almost exclusively among kin and explains the common but uncharacterized phenomenon of genotype spatial segregation in infected plants.

Viral populations can evolve rapidly, even during a single host infection, and the resulting changes in the population ultimately can affect the outcome of viral diseases. A clear example of this is the emergence of drug-resistant mutants of animal/human viruses, of resistance-breaking variants of plant viruses, or of recombinant genotypes with an enlarged host range. Therefore, it is not surprising that increasing efforts are being made to characterize parameters defining within-host evolution of viral populations.

Since viruses are obligate intracellular parasites, a fundamental parameter determining their within-host population dynamics/genetics is the multiplicity of cellular infection (MOI), defined as the number of genomes of a given virus species that infects a cell. The MOI influences two major processes in viral evolution, namely, the population bottlenecks and the interactions among genotypes. Within-host bottlenecks are linked to the number of infected cells during host colonization and to the MOI at which these cells are infected. The overall intensity of interactions among viral genomes, i.e., competition, genetic exchange, functional complementation, and collective action, depends to a large extent on the probability of encountering different genotypes within host cells, a probability that is directly linked to the MOI. Given the impact of the MOI on these key processes, many theoretical and empirical studies using cell cultures have directly explored the impact of different MOI regimens on virus evolution (1–8). These studies show that proceeding as a single genome or as a group of genomes during cell infection can largely influence viral fitness and virulence.

It is remarkable that many unrelated viruses can prevent secondary infections of cells by closely related genotypes (9–18). In these cases of "superinfection exclusion," different viral genotypes coinfecting a host are rarely found coinfecting cells, and they sometimes segregate into distinct groups of cells or tissues within

Received 27 February 2015 **Accepted** 8 July 2015

Accepted manuscript posted online 15 July 2015

Citation Gutiérrez S, Pirolles E, Yvon M, Baecker V, Michalakis Y, Blanc S. 2015. The multiplicity of cellular infection changes depending on the route of cell infection in a plant virus. J Virol 89:9665–9675. doi:10.1128/JVI.00537-15.

Editor: A. Simon

Address correspondence to Stéphane Blanc, blanc@supagro.inra.fr.

* Present address: Serafín Gutiérrez, Control of Exotic and Emerging Animal Diseases Unit (CMAEE), CIRAD, Montpellier, France.

doi:10.1128/JVI.00537-15

which only one genotype is observed (19–25). Superinfection exclusion and spatial segregation of genotypes has been observed in some host-virus models but not in others (26), suggesting inconstant or different mechanisms for the control of cell infection among viruses.

Understanding such contrasting cell coinfection patterns is important because they lead to different predictions on the composition, spatial structure, and evolution of viral populations within a host. Unfortunately, thus far, formally connecting these coinfection patterns to distinct MOIs is difficult due to the paucity of data. The MOI has been quantified in only a few multicellular host-virus models: an insect virus (27), an arbovirus in its mosquito vector (28), four plant viruses (each in a different host) (26, 29–32), and HIV (33–35). In all cases the estimated values ranged from one to a few genome units per cell, suggesting that the MOI generally is low. Beyond this small number of reports, the current view is biased by the fact that, in both theoretical and experimental studies in cell culture, the MOI has been oversimplified and set as a constant value during the infection cycle. Nevertheless, MOI changes during host invasion recently have been observed in two distinct virus models: (i) the MOI of *Cauliflower mosaic virus* (CaMV) can increase from 2 to 13 genomes per cell in successively colonized leaves (26), and (ii) the MOI of HIV in $CD4^+$ blood cells increases during the late chronic phases of the infection (33).

Here, we present a detailed analysis of the MOI of an RNA virus, *Turnip mosaic virus* (TuMV; genus *Potyvirus*), during infection of turnip plants. We analyzed the colonization of the host compartments most important for the virus cycle (i.e., sieve tubes, companion cells, mesophyll, and epidermis) and at different time points during infection. Our results show that the MOI is below one genome per cell in companion cells primarily infected from the vasculature, resulting in the coexistence of several clonal lineages initiated from distinct infection foci within a single leaf. The MOI then sharply rises to several tens of genomes per cell when these lineages progress into the mesophyll through cell-to-cell movement, allowing intense interactions between kin viral genomes. We also observed a marked spatial segregation of two genetically labeled genotypes of TuMV, showing that lineages that initiated independently within a leaf rarely coinfect cells later, despite high MOIs in the mesophyll. Here, we explain this observation by showing that numerous TuMV genomes can enter and infect the same mesophyll cell, but that this is possible for only a very short time due to the rapid onset of an unknown but very efficient mechanism of superinfection exclusion.

MATERIALS AND METHODS

Plasmid constructions. We generated TuMV clones expressing either mGFP5 or mRFP1 tagged with a nuclear localization signal (NLS). This modification concentrated fluorescence in nuclei, facilitating identification of infected cells and limiting free diffusion of fluorescence proteins between cells. The sequences of all primers used to create the clones are available upon request. The QuikChange site-directed mutagenesis kit (Stratagene) was used to insert a single copy of the NLS of the large T-antigen protein of simian virus 40 (36) right after the coding region of mGFP5 in the plasmid p35Tunos/cGFP (37) to create p35Tunos/cGFP-NLS. This plasmid contains the entire sequence of TuMV-UK1 with mGFP5-NLS inserted between the viral genes NIb and CP. The mGFP5-NLS coding sequence in this construction is flanked by NIa proteolytic cleavage sites, inducing the release of free mGFP5-NLS from the TuMV polyprotein. The coding sequence of the nucleus-targeted mGFP5 then was replaced by the mRFP1 gene (Clontech) to create p35Tunos/cRFP-NLS. This was performed using the megaprimer method and the site-directed mutagenesis kit from Stratagene. To create agroinoculation-infectious clones, full TuMV genomes of both p35Tunos/cGFP-NLS and p35Tunos/cRFP-NLS were excised through digestion with SmaI and ApaI and inserted in SmaI/ApaI-linearized pCambia0390, generating pCambia-tunos/cGFP-NLS and pCambia-tunos/cRFP-NLS.

Aphid rearing, plant growth conditions, and virion purification. Colonies of the aphid species *Myzus persicae* were reared on eggplant as previously described. Turnip plants (*Brassica rapa* cv. Just Right) were maintained in an insect-proof growth chamber under controlled conditions (temperature, 24/15°C; photoperiod 15/9-h day/night). TuMV virions were isolated from turnip plants 20 days after agroinoculation with either the green fluorescent protein (GFP) clone or the RFP clone and using a combination of the methods of Murphy et al. and Sako (38, 39).

Inoculation and sampling. Plantlets at the third leaf stage were mechanically inoculated with virion suspensions or agroinoculated with the above-described pCambia plasmids. For both inoculation methods, inocula consisted of a mixture of the GFP and the RFP clones at a 1:1 ratio, verified using reverse transcription-quantitative PCR (RT-qPCR) or optical absorbance of bacterial suspensions. Mechanical inoculation was carried out by rubbing a virion suspension containing 1 μg of virus particles and Carborundum abrasive powder on the second leaf level. Agroinoculation was performed as previously described (40).

The appearance of new leaves (budding) on the inoculated plants was monitored and noted daily in order to allow leaf sampling at a precise leaf age. Six leaf discs (0.8-cm diameter) distributed evenly over the leaf surface were sampled for each leaf. In some experiments, whole leaves were collected instead (indicated in the text). RNA from individual leaf samples was extracted using the RNeasy plant minikit (Qiagen) by following the manufacturer's instructions.

During the growth of turnip host plants, leaves appear successively to develop a rosette. Leaves can be numbered according to their order of appearance, and the first leaf of each plant corresponds to leaf level one in a plant set, the second to leaf level two, and so on. When considering a leaf of a single plant, we usually indicate its leaf number (1st leaf, 2nd leaf, 3rd leaf etc.), whereas when considering a whole plant set the term leaf level is used, which corresponds to an ensemble of leaves with the same leaf number.

RT-qPCR. All primers used for qPCR and RT-qPCR are available upon request. For each sample (either plant or aphid RNA extracts), reverse transcription was carried out using avian myeloblastosis virus (AMV) reverse transcriptase (Promega) by following the manufacturer's specifications. cDNAs then were diluted 1/10, and two microliters were used as the template in a real-time qPCR with the LightCycler 480 SYBR green I master (Roche) in a LightCycler 480 thermocycler (Roche). The PCR program for virus quantification was 95°C for 10 min, 45 cycles of 95°C for 15 s, 65°C for 15 s, and 72°C for 15 s, and then a melting curve analysis. The program for quantification of the actin transcript was identical except for the annealing temperature (62°C instead of 65°C). Different primer pairs were used to estimate virus copy number in plants and in aphids due to specificity problems.

PCR fluorescence data were analyzed using LinReg software (41). Plasmid dilutions containing the full genome of each TuMV clone or the *B. rapa* actin gene provided standard curves, which were used to estimate and compare the virus copy number in aphids or the normalized virus copy number per actin transcript in plant leaves, respectively. The *mrfp1* frequencies in each of the samples were calculated by dividing the number of *mrfp1* copies by the sum of the number of copies of both *mrfp1* and *mgfp5*.

Marker neutrality. Forty plants were inoculated in parallel with a virion suspension containing a 1:1 mixture of the two genotypes. Five leaf levels (levels 6, 11, 16, 21, and 27) were sampled, each at a different time during infection, in all of the plants. All leaf levels were sampled at 13 days of development, when the sink-to-source physiological transition had already taken place and leaves generally were fully infected. The inoculated

leaf also was sampled just before its senescence. For each sampled leaf, RNA was isolated and the relative frequency of the mRFP1 and GFP5 clones estimated with quantitative RT-PCR.

Recording of spatial segregation during infection of a leaf. Twelve plantlets were agroinoculated with a 1/1 ratio of the two genotypes on the 2nd and 3rd leaves. mRFP1 and mGFP5 fluorescence levels in leaf level 7 (the second systemically infected leaf level) were scanned 10 times in 15 days (at days 7, 8, 9, 10, 11, 15, 17, 18, 21, and 22 after appearance on the plant) in all of the plants. Analyses of the same leaves along a time course was possible because the plants had been potted in containers, allowing us to place plants in a Typhoon FLA 9000 scanner (GE Healthcare Life Sciences) and to scan the fluorescence of uncut leaves. Excitation wavelengths of mGFP5 and mRFP1 were 473 nm and 532 nm, respectively. Filters for mGFP5 and mRFP1 fluorescence acquisition were BPB1 (530DF20 nm) and BPG1 (570DF20 nm), respectively. Pixel size was set to 50 μm. A white-light image of each leaf was taken at the last sampling point. Observation with confocal microscopy of sites coinfected by both the GFP and RFP clones was done with an LSM700 confocal microscope (Zeiss). mRFP1 was excited with a 555-nm LED laser, and the mirror was set to record emission from 555 to 620 nm. mGFP5 was excited with a 488-nm LED laser, and emission was collected from 490 to 530 nm.

Estimation of the MOI during primary leaf infection when the virus exits sieve elements. Leaf level 7 was examined in six plants from the above-described experiment by recording spatial segregation during the infection of a leaf. Fluorescent foci of the three possible types (GFP, RFP, or dual fluorescence) were counted in the images obtained at day 7 after appearance of leaves on the plant, the first time point of the previous experiment (for an example, see the first image in Fig. 2A). Only discrete patches with a rounded shape and a small size were counted to avoid patches derived from coalescence of more than one initial infection focus. The average MOI in the cells that initiated each of these foci was estimated using the methodology previously described (26), with estimates of the frequency of patches showing dual fluorescence, the frequency of each fluorescent variant in the leaf (calculated from the respective number of patches with a specific fluorescence), and the total number of patches counted in each leaf.

Estimation of the MOI during ulterior cell-to-cell movement. Three separate sets of plants were inoculated with a virion suspension (1:1 mix of the two genotypes) on leaf level 1. Each set consisted of 40 to 60 plants. Inoculated leaves were collected 4 days after inoculation. At this time point, fluorescent circles indicative of infection foci are easily visualized on the leaves under the microscope. Preliminary experiments had shown that few infection foci derive from systemic infection at the selected time point and that the inoculum dose was close to saturation (not shown). mRFP1 and GFP5 fluorescence was scanned on whole leaves using a Typhoon FLA 9000 scanner (GE Healthcare Life Sciences) as described above. After scanning, leaves were kept between humidified paper for further analysis with confocal microscopy. Images were immediately analyzed for foci with total or partial colocalization of the two fluorescence channels. Confocal microscopy images of the detected coinfected foci then were taken using an LSM700 confocal microscope (Zeiss) as described above. In all cases of coinfected foci, the actual colocalization of the two TuMV genotypes within individual cells was ascertained by scrutinizing optical sections provided by confocal microscopy. The model developed to infer the MOI during cell-to-cell movement from these observations is described in Results.

Time to activate superinfection exclusion. Three systemically infected leaves, each from a different plant, were collected when they had reached their 13th day of development. Leaves were observed under confocal microscopy, and images of frontiers between two patches of infected cells, each patch showing a different fluorescence, were taken as described above. For each of the three collected leaves, six such frontiers were analyzed. As shown in Fig. 1G, a line was drawn along the frontier, and 4 to 6 additional perpendicular lines were drawn at a 100-μm interval (only one perpendicular line is shown in Fig. 1G; the cell diameter is around 40 μm) using ImageJ software (42). Cells showing the two fluorescence channels in confocal optical sections were counted on lines perpendicular to the frontier.

To determine the speed of cell-to-cell movement, leaf level 1 was inoculated with a virion suspension in 20 plants in parallel. Plants were potted in containers, allowing us to place them in a Typhoon FLA 9000 scanner (GE Healthcare Life Sciences). Fluorescence on the inoculated leaf was scanned at 3 and 4 days postinoculation as described above. The diameter of 247 foci at both sampling dates was estimated on the images and used to determine the number of cell-to-cell movements in 24 h.

Estimation of viral load in sap. Quantification of viral load in sap during infection was performed as previously described (43), with modifications. Briefly, the method is based on the fact that *Myzus persicae* aphids engaged in sustained feeding on phloem sap containing freshly collected sap within their gut that is constantly renewed. Thus, the viral load in the sap flowing into a young leaf at a given time point can be estimated through the quantification of the viral load in aphids. Using this method, we estimated the viral load in five leaf levels (leaf levels 6, 11, 16, 21, and 27) that appear consecutively on the plant during infection.

One hundred plantlets were mechanically inoculated with a virion suspension. At each of the 5 sampling points (one per leaf level analyzed), 20 plants were randomly drawn and 90 *M. persicae* aphids per plant were caged on the selected leaf level. The selected level always had 5 days of development before sampling. At this age, leaves have not yet gone through the sink-to-source transition and phloem sap flows into them. Three groups of 10 aphids were collected from each of the 20 leaves after 10 min on the leaf, a period during which aphids probe leaf cells but do not feed from the phloem. The same caged populations again were sampled using the same protocol after an overnight feeding period, a period long enough to allow continuous phloem feeding. The whole leaf also was collected and its RNA extracted. Plants then were discarded. RNA from each group of 10 aphids was isolated using the RNeasy minikit (Qiagen). Viral load in aphids and in leaves was quantified using quantitative RT-PCR as described above.

Spatial segregation of and cell coinfection by the GFP and RFP clones in different leaf levels. Twenty plantlets were agroinoculated as described above. mRFP1 and mGFP5 fluorescence channels in five leaf levels (levels 6, 11, 16, 21, and 27) were recorded when leaves were 13 days old in all of the plants. For each level, leaves were collected and their fluorescence scanned with a Typhoon FLA 9000 scanner (GE Healthcare Life Sciences). For each leaf, several parameters were estimated using the ImageJ macro "Leaf Infection Tools" (http://dev.mri.cnrs.fr/wiki/imagej-macros/Leaf_Infection_Tools). The estimated variables were total surface, mRFP1 and mGFP5 surface, and surface with colocalization of both fluorescence channels.

RESULTS

Two fluorescently labeled TuMV clones spatially segregate in infected leaves. To easily visualize cell coinfection and spatial segregation, we adapted an approach successfully reported for other plant RNA viruses (19, 24). We created two TuMV clones only differing in an allelic sequence coding for a fluorescent protein, either mGFP5 or mRFP1. We first confirmed the equicompetitiveness of the two clones by monitoring their relative frequencies in 20 plants coinfected in parallel on six successive leaf levels (Fig. 1A). The relative frequency of the two clones did not significantly change in the plant set over time (linear mixed-effect model on the relative frequency of one genotype with leaf level as a fixed effect and individual plant as a random effect [$F_{6,\ 192} = 1.877$, $P = 0.086$]), indicating that the two clones are equicompetitive in our experimental conditions. In a new, similar plant set, we next analyzed their respective distributions in infected tissues. Because an NLS peptide is fused to the reporter proteins to prevent passive diffusion into neighboring cells, the fluorescence

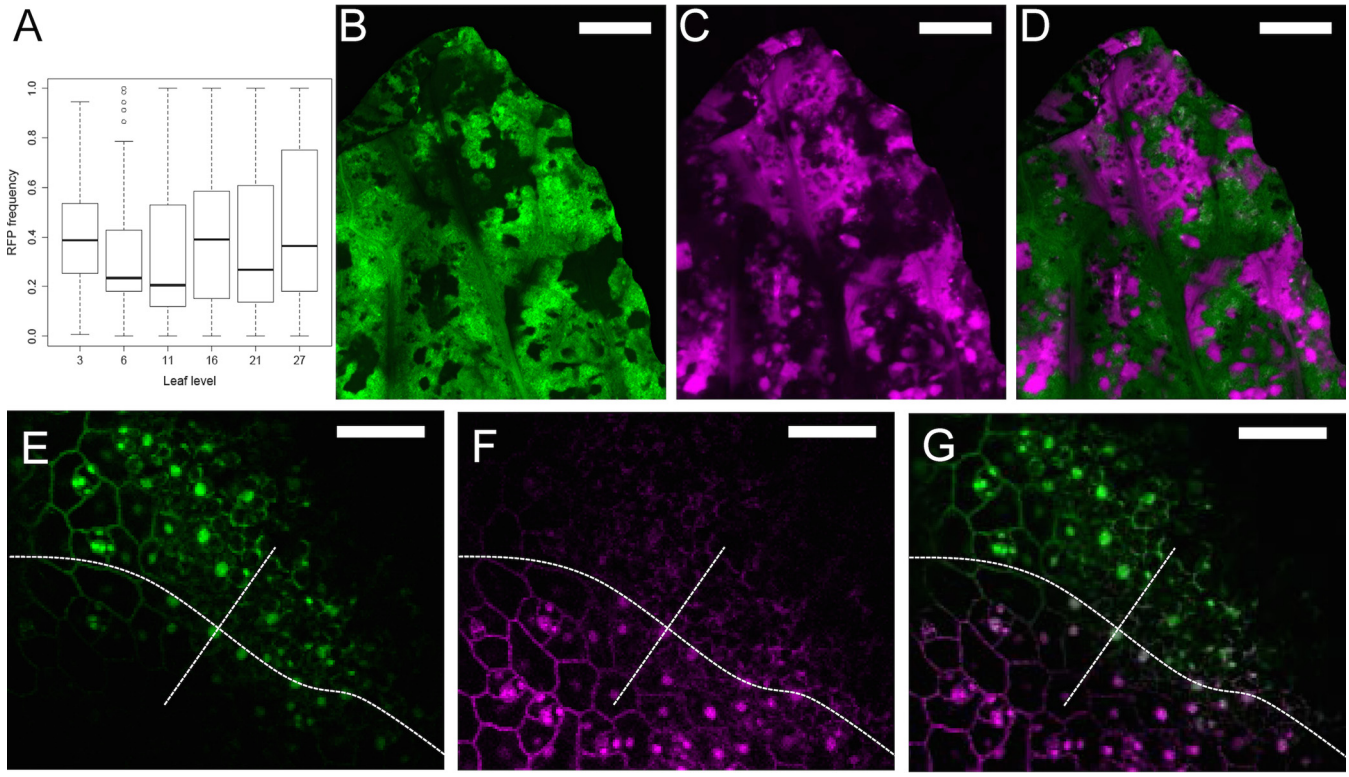

FIG 1 Spatial segregation of TuMV genotypes expressing fluorescent proteins in a leaf. (A) Relative frequency of the mRFP1 clone in different leaf levels of 20 turnip plants coinoculated in parallel with mRFP1- and mGFP5-expressing TuMV clones. Each leaf level except that of the inoculated leaf (leaf level 3) was sampled at the same age (13 days after apparition on the plant). Relative frequencies were calculated as the number of copies of the mRFP1 clone divided by the sum of the copies of mRFP1 and mGFP5 clones. The variations of the relative frequency of the two clones across leaf levels was not significant (statistical analysis is detailed in the text), indicating that the two clones are equally competitive in our experimental conditions. (B and D) Detail of a leaf coinfected by the mGFP5- and the mRFP1-expressing TuMV clones. Epifluorescence images were recorded with a Typhoon FLA 9000 (bar, 0.5 cm). The GFP channel (B), the RFP channel (C), and a merge image of both channels (D) are shown. mGFP5 and mRFP1 fluorescence rarely overlap, indicating spatial segregation. (E to G) Frontier between two infection fronts in a leaf viewed with confocal microscopy (bar, 50 μm). Optical sections of the GFP and RFP channels and merge images (E, F, and G, respectively). Fluorescence is readily visible in the nuclei of cells. The curved lines indicate the frontier between two infection fronts, and the perpendicular lines across the curved lines are used to guide the counting of the number of cells where the two fluorescent genotypes colocalize in the nucleus.

of RFP and GFP concentrated in the nuclei of infected cells and could easily be distinguished both at the tissue and cell levels (Fig. 1B to G).

Although the two clones coinfected individual plants, they colonized distinct territories within each leaf, leading to a patchwork distribution of mGFP5 and mRFP1 fluorescence, a phenomenon earlier described for several plant viruses and often referred to as spatial segregation (Fig. 1B to D). We believe that two successive phenomena are at the basis of spatial segregation, irrespective of plant virus species. First, the two viral clones that move long distances in the same veins must separate when initiating infection foci in systemically infected leaves. Second, superinfection exclusion must preclude remixing of the clones during expansion of the various infection foci through cell-to-cell movement. With these simple conditions, the genotypes separated when exiting the vasculature would progress cell to cell into healthy tissues and be arrested when encountering previously infected territories. To investigate this process in further detail, we report here (i) a quantitative approach to estimate a very low MOI in companion cells during initial loading of the virus from sieve tubes, (ii) quantitative estimates of the MOI in mesophyll/epidermis during subsequent cell-to-cell movement, and (iii) the efficiency and timing of the inhibition of secondary infection.

Leaf cells primarily infected from the vasculature are infected at low MOI. We monitored the distribution of mGFP5 and mRFP1 fluorescence during systemic invasion of a single developing leaf. Our goal was to visualize how spatial segregation was established and potentially maintained during leaf infection and development. Fluorescence was scanned daily in the 7th leaf of a plant (one of the first leaf levels to be fully systemically infected) for a 15-day period spanning from early stages of leaf development to full maturity. The experiment was repeated on 12 plants infected in parallel, and one representative plant is shown in Fig. 2. Due to natural and virus-induced wrinkling of the leaves, some leaf regions (mainly those close to the main vein) were not always in contact with the screen during scanning, hampering the recording of fluorescence in these specific areas.

Fluorescence, indicative of infection, was already present at the first sampling point (at 14 dpi), when the young leaves were 7 days old (Fig. 2A). Fluorescence first appeared in patches close to veins that later increased in size until most of the leaf surface became infected when the leaf was 11 days old. We clearly observed the establishment of spatial segregation, and once established, this phenomenon did not revert or further evolve within a leaf. The distribution of the mGFP5 and mRFP1 fluorescence remained nearly identical after day 9 (Fig. 2A, compare days 9, 10, and 11),

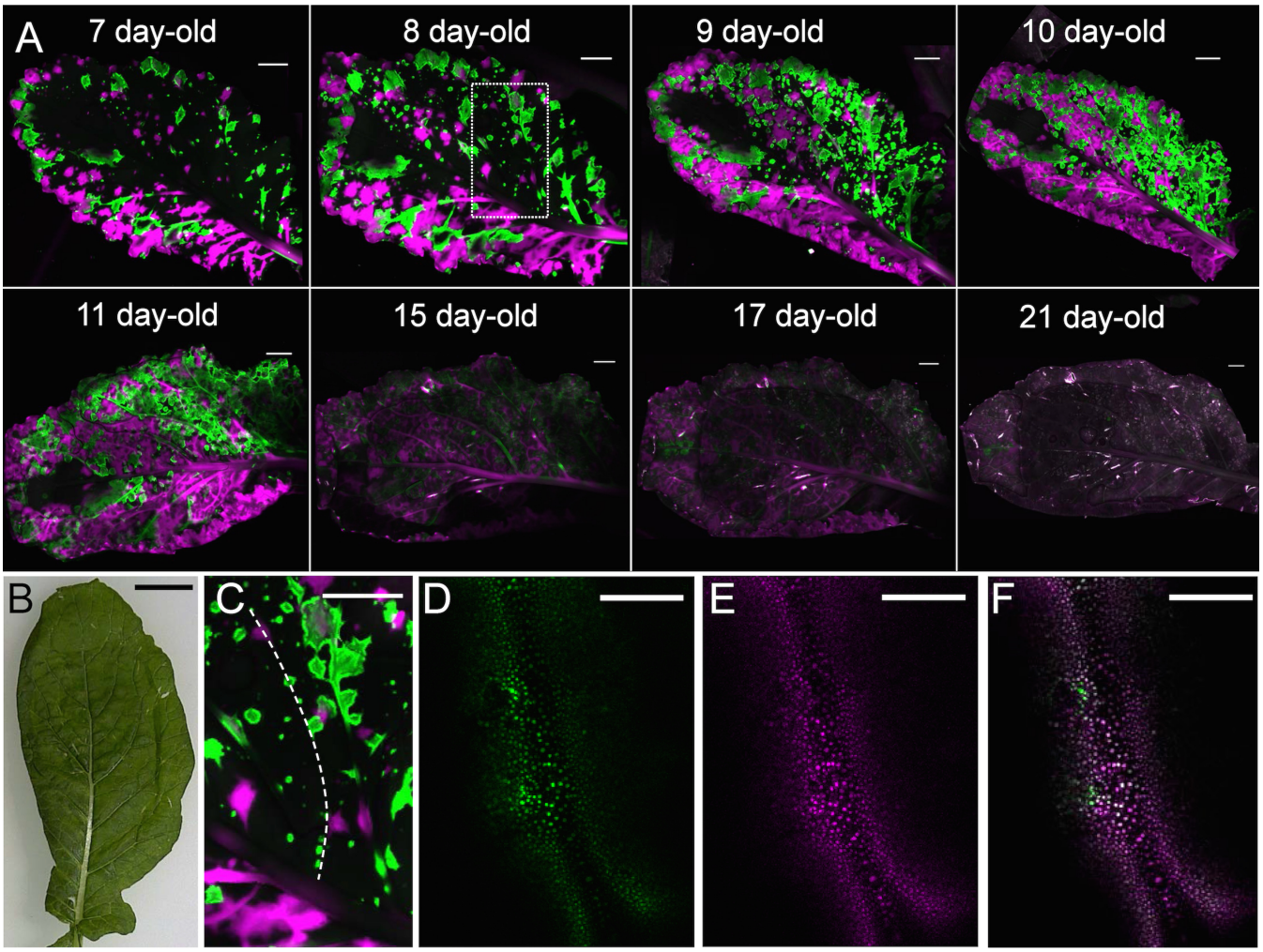

FIG 2 Systemic infection of a leaf by TuMV clones expressing fluorescent proteins. (A) Time course analysis of the fluorescence in a leaf systemically infected by two TuMV clones, each expressing a fluorescent protein (mGFP5 in green and mRFP1 in magenta). The 8 images are epifluorescence-merged images of the RFP and GFP channels recorded at the indicated time points, during the life of the same leaf, with a Typhoon FLA 9000 (GE Healthcare Life Sciences). The virus-induced fluorescence totally disappeared from day 15 on. At these late points, images were taken with a higher photomultiplier voltage to be able to visualize the leaf through its autofluorescence. The inset from day 8 is enlarged in panel C. (B) At day 21 the leaf is not senescent, as shown here with visible light, although some damage due to repeated manipulation is visible (bar, 2 cm). (C) The dotted white line follows a vein to facilitate estimation of the distance between infection foci on the same vein (bar, 0.4 cm). (D to F) One of the rare primary infection foci appearing along veins where the two fluorescent genotypes colocalized (bars, 200 μm). Optical sections obtained with confocal microscopy of the GFP (D) and RFP (E) channels and merge images (F).

until the overall virus-related fluorescence decreased to a point where it was barely distinguishable from leaf autofluorescence (Fig. 2A, compare days 7 to 11 to days 15 to 21). Interestingly, this total loss of virus-related fluorescence did not correlate with leaf senescence (Fig. 2B), signs of which could not be observed before an additional period of 7 days or more (at least after day 24) (not shown). Since the TuMV genome is translated as a single large polyprotein, all gene products (including reporter fluorescent proteins) are generated together. Thus, the decay in virus-related fluorescence suggests that viral protein expression stopped before day 15, long before leaf senescence and cell death.

At early time points, the infected foci were observed along the veins. We immediately noted that isolated foci showed a single fluorescence (Fig. 2A and C), except in rare instances shown in Fig. 2D to F and further discussed below. The distance between initial foci on the same vein could reach up to 0.5 cm (Fig. 2C), suggesting that the entry of the virus occurs in a limited number of cells. Because companion cells are densely packed all along sieve elements within veins, these qualitative results strongly suggest two phenomena: (i) a low rate of infection of companion cells from virus navigating in the vasculature, and (ii) infection of these companion cells with a single viral genome on average, as attested by a single fluorescence in the immense majority of the observed foci. Please note that in the vein regions away from infection foci, we could not detect any fluorescence in companion cells, confirming that they are rarely infected.

Six plants out of this plant set were used to analyze and count 377 infection foci along the leaf veins and to estimate the MOI at this early stage of the infection cycle as described in Materials and Methods. Only six coinfected foci were observed out of the 377 counted (frequency of coinfected foci per leaf, 0.018 ± 0.013 [means ± standard deviations {SD}]). The average MOI calcu-

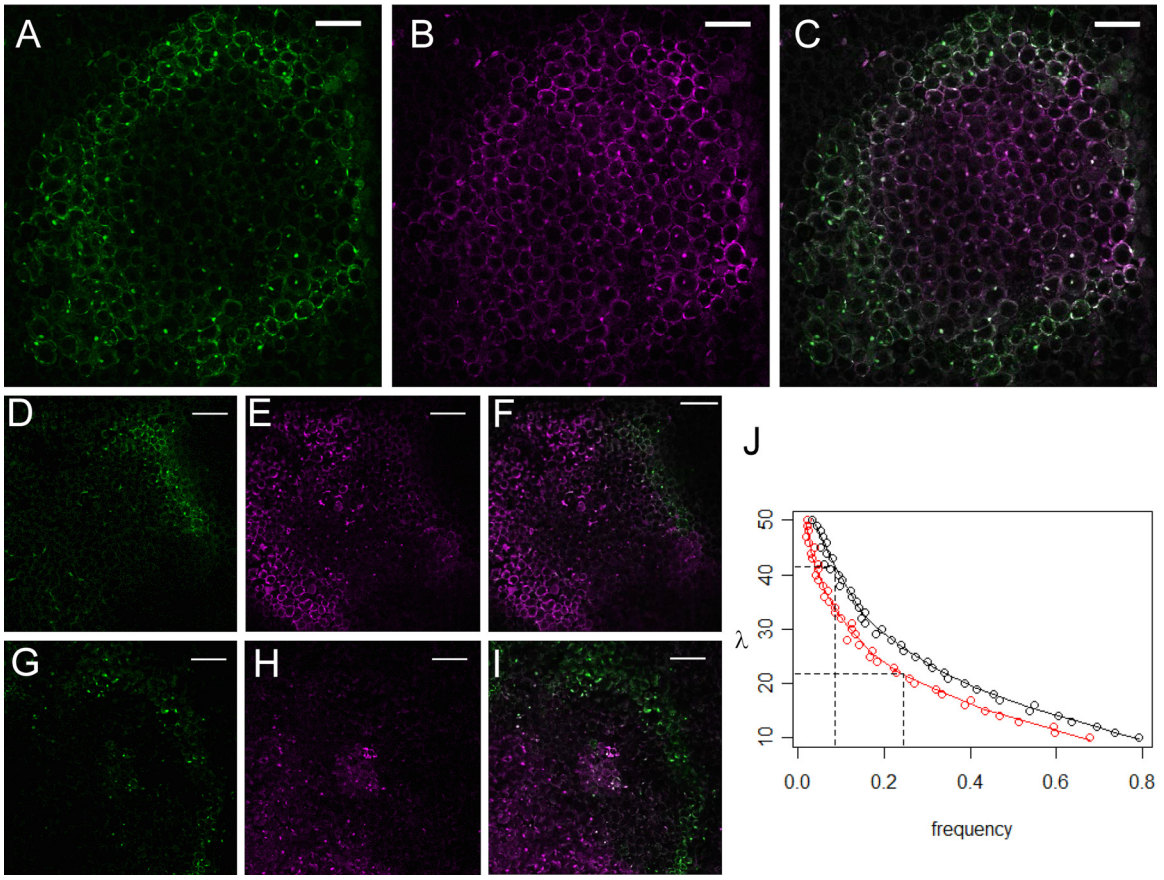

FIG 3 Analysis of the MOI during cell-to-cell movement of TuMV. (A to C) An optical section of an infection focus, visualized under confocal microscopy 4 days after mechanical inoculation of a virus suspension on a leaf. Colocalization of the two types of fluorescence can be observed all over the foci (bars, 100 μm), although with variable intensity in the inner and outer parts, which might be due to distinct maturation and turnover time for the two fluorescent proteins produced in plant cells. Single-channel images in GFP (green) (A) and RFP (magenta) (B) channels and a merge image (C). (D to I) Same as panels A to C, but this time images were taken from two distinct foci (D to F and G to I, respectively) where sectors showed a single fluorescence (bars, 200 μm). (J) Estimation of the MOI during cell-to-cell movement through simulations. MOI values (*y* axis) versus the probability of losing a marker after 13 (red circles) or 16 (black circles) cell-to-cell movements (*x* axis). Locally weighted scatterplot smoothing (LOWESS function, R software) was used to fit a curve to the data and to graphically estimate MOI values (full lines). The dotted lines indicate the MOI values for which there is a probability of losing one marker of 0.085 after 13 cell-to-cell movements or a probability of losing a marker of 0.245 after 16 cell-to-cell movements.

lated from these primary infection sites was estimated to be 0.072 (95% confidence interval [CI], 0.029 to 0.146), further confirming that most foci were initiated by a single genome.

High MOI during cell-to-cell movement. Confocal microscopy analysis of the very rare primary infection foci that exhibited both fluorescence channels provided an unexpected result. In these cases, when the two genotypes coinfect a cell, one of the fluorescent alleles should be rapidly lost if the MOI is low during subsequent cell-to-cell movement. We did not observe such a fluorescence loss, despite the fact that infection sometimes had progressed up to 30 cell-to-cell movements from the vein (Fig. 2D to F), indicating that the MOI during subsequent cell-to-cell movement must be high enough to maintain both clones.

To formally quantify the MOI during cell-to-cell movement, we used an approach similar to that of Miyashita and Kishino (30). This approach is based on the fact that when a population goes through periodic genetic bottlenecks between generations, the size of these bottlenecks defines the speed of fixation of neutral alleles in the population. During leaf colonization by TuMV, we assumed that a new generation takes place at each cell-to-cell movement. Under this assumption, the probability of fixation of one of the fluorescent markers in our TuMV population during cell-to-cell movement depends on the MOI: the lower the MOI, the faster the fixation of one of the genotypes in the population.

We mechanically inoculated leaves with a highly concentrated suspension of purified virions containing a mixture of equal amounts of mGFP5- and mRFP1-expressing TuMV. This method generates distinct infection foci all over the leaf (local lesions), and most foci originate from the infection of a single cell. Foci generally showed a rounded shape at 4 days after inoculation (Fig. 3A to C), and the number of concentric cell layers from the center to the border of the foci was 14 cells on average at this time point (95% CI, 13 and 16). Later, infection often reached veins leading to foci with asymmetric shapes (not shown). In order to look for rare doubly infected foci, we scanned the fluorescence at 4 days after inoculation in three replicate experiments of around 50 leaves each. We analyzed 3,240 foci in total, among which only 85 exhibited dual fluorescence (2.7%). The absence of doubly infected cells in the center of the 3,155 foci with a single fluorescence (not shown) was carefully checked by examining the cell nuclei in optical sections as shown in Fig. 3A to C.

We then analyzed whether there were sectors (groups of cells) containing a single kind of fluorescence in each of the doubly infected foci. Such sectors would result from the loss of one of the fluorescent genotypes in the population that progresses from cell to cell (29). We only identified 14 out of 85 foci (16.5%; 95% CI, 8.5% to 24.5%) presenting a sector with only one fluorescence type, indicative of fixation of one of the genotypes in the sector (Fig. 3D to I). Those foci presented two distinct patterns of fluorescence distribution. In 12 out of the 14 foci, the focus was divided in two sectors, each with a single fluorescence (Fig. 3D to F). In the two remaining foci, two sectors were visible: one showed coinfection, whereas the other showed a single type of fluorescence (Fig. 3G to I). These patterns of fluorescence distribution could be the result of two foci initiated in distinct neighboring cells instead of a focus initiated in a single coinfected cell. Since we could not distinguish between the two situations (single focus versus two foci in contact) and in order to provide a conservative conclusion, we included all such foci in the analysis.

To quantify the MOI using the parameters estimated as described above and their variability, we simulated the cell-to-cell progression of a virus population in a linear array of cells. In our simulation, each cell is infected from a virus population issuing from a single cell, the previous one in the series. The rationale and implications of this simplification are detailed in Discussion. In our simulation, cell 0, the first cell in the series, is inoculated with two genomes, one of each type. A viral population of 1,000 genomes then is generated within the cell by random sampling of the infecting genotypes. An MOI value next is randomly drawn from a zero-truncated Poisson distribution of mean λ, and the corresponding number of viral genomes is drawn from the population in cell 0 and transferred to cell 1. If one genotype is lost during the transfer, the infection series is arrested at cell-to-cell transfer 1; otherwise, the infection similarly progresses from cell to cell until a defined number of cells is reached. Simulations were run with two maximal numbers of cell-to-cell movements corresponding to the observed 95% CI of the average numbers of cell-to-cell movements 4 days after inoculation (13 and 16, as indicated above). This simulation allows stochastic processes to take place during both replication and movement.

We used a range of λ values from 1 to 100 to determine the probability of losing an allele after a given number (n) of cell-to-cell movements (max_n; either 13 or 16) (Fig. 3J). For each λ value and max_n, we performed 10^6 simulations and recorded the frequency at which fixation had occurred. Using locally weighted scatterplot smoothing (44) (LOWESS function, R software), we then fit a curve through the data and estimated a conservative 95% CI of λ, which corresponded to the MOI of TuMV during cell-to-cell movement in the mesophyll. We determined the maximum λ value as that leading to the lowest 95% CI of the observed probability of fixation (0.085) after the largest 95% CI of the observed number of cell-to-cell movements (16); this gives an MOI upper value of 41.5. Similarly, we determined the minimum λ value as that leading to the highest 95% CI of the observed probability of fixation (0.245) under the smallest 95% CI of the observed number of cell-to-cell movements (13); this gives an MOI lower value of 21.7.

Superinfection exclusion operates shortly after cell infection. The high MOI estimated during cell-to-cell movement should facilitate multiple infections of cells by different genotypes. However, across a whole leaf, the rate of cell coinfection by the two fluorescent clones was low (Fig. 1 and 2). As indicated earlier, this low coinfection rate could be due to the initial separation of the two genotypes resulting from the low MOI in companion cells from the vasculature, associated with a mechanism of superinfection exclusion. Such a mechanism could rapidly develop and prevent extensive secondary mixing of the genotypes when their respective infection fronts come into contact, even if the MOI is high at this point. Thus, we set up a protocol to determine the time required for the onset of superinfection exclusion in cells infected by TuMV.

To estimate the speed of cell-to-cell movement on the infection front, we determined the average time to infect a new cell during radial growth of foci between 3 and 4 days after mechanical inoculation. The speed of cell-to-cell movement of TuMV was calculated from 247 infection foci (local lesions) from a total of 20 different inoculated leaves, each from a different plant, as described in Materials and Methods. The infection front advanced with an average speed of 2.94 ± 0.97 h/cell (means ± SD).

We then estimated the number of cell-to-cell movements that a genotype can actually make when entering into an area already infected by another. This information can be obtained by counting the number of cells that express both types of fluorescence at the junction between mGFP5 and mRFP1 territories within a leaf (an example is depicted in Fig. 1E to G). After defining a line of cells as the approximate frontier between the two patches, we measured the number of cells showing dual fluorescence in lines perpendicular to the frontier line (Fig. 1G). The number of coinfected cells found along these perpendicular lines was 1.71 ± 0.92 (means ± SD) on each side of the frontier. Thus, superinfection exclusion appears to be activated and fully effective in less than 6 h, a lapse during which the virus can undergo two successive cell-to-cell movements at most. We made this estimate in leaves that are 13 days old, where the infection is fully developed, and where the infection fronts and the color patches do not further advance or evolve, as shown in Fig. 2 and further confirmed in the next section.

Spatial segregation is maintained during infection. The observed spatial segregation of the two TuMV genotypes in systemically infected leaves relies on their initial separation when entering leaf tissues, i.e., at an MOI close to one genome per cell in primarily infected companion cells. We hypothesized that this low MOI results from a low TuMV titer in the sap flowing into the leaves at early infection stages. The question was whether the TuMV load in the sieve tubes could increase when infection progresses into upper leaf levels and whether this could later lead to higher MOIs in primarily infected cells and to relaxed spatial segregation of the two clones. To address this, we monitored the viral load in sap through time, in parallel to the establishment of spatial segregation, in successive leaf levels appearing during TuMV infection (Fig. 4 and 5).

The TuMV load in the phloem sap was evaluated as previously described for CaMV, for which aphids were used as pure-sap collection devices (43). We analyzed phloem sap in young sink leaves (when leaves were 5 days old) from five successive leaf levels of 20 plants infected in parallel. For each individual leaf, we determined the viral load in aphids after an overnight period of sustained feeding into the sieve tubes. Figure 4A shows that the TuMV sap load significantly changed during infection (linear mixed-effects model with leaf level as fixed effect and plant as random effect; $F_{4,\ 68} = 4.709$; $P = 0.002$), but that this change was limited and

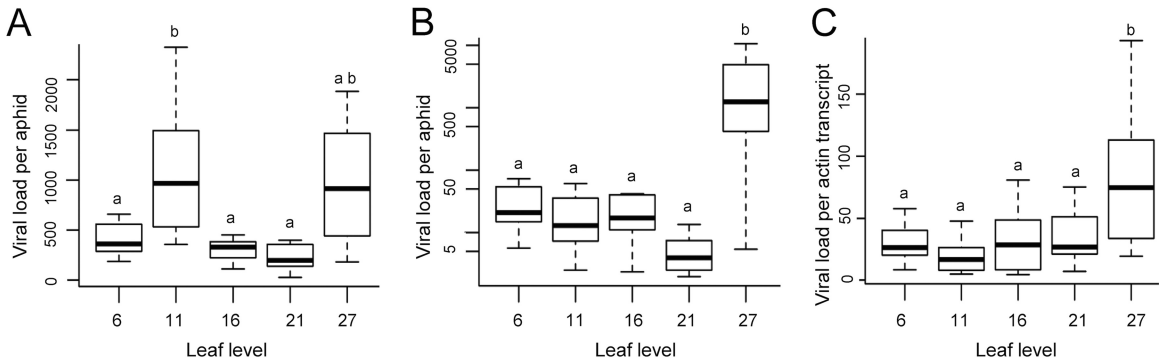

FIG 4 Dynamics of the viral load in sap of TuMV-infected turnip plants. (A) Viral load per aphid in aphids having fed overnight on different leaf levels after subtraction of the viral load in aphids having fed for 10 min in parallel on the same leaf levels. (B) Viral load in aphids having fed for 10 min on a given leaf level (*y* axis in log scale). (C) Viral load (copies of virus genome per copy of actin mRNA) in the leaves on which aphids fed. Letters indicate significant differences.

remained in the same order of magnitude, from a few hundred to around a thousand virus genomes per aphid.

As controls, we also estimated the viral load in short-fed aphids (feeding for a few minutes on epidermis and mesophyll) and directly in the leaf extracts (mainly mesophyll cells). The TuMV load in short-fed aphids generally was 100 times lower than that in long-fed ones (compare Fig. 4A to B), and the dynamics of the viral load between the two treatments was significantly different (linear mixed-effect model with treatment and leaf level as fixed effects and plant as random effect; $F_{1,\,3,\,159} = 76.677$; $P < 0.0001$),

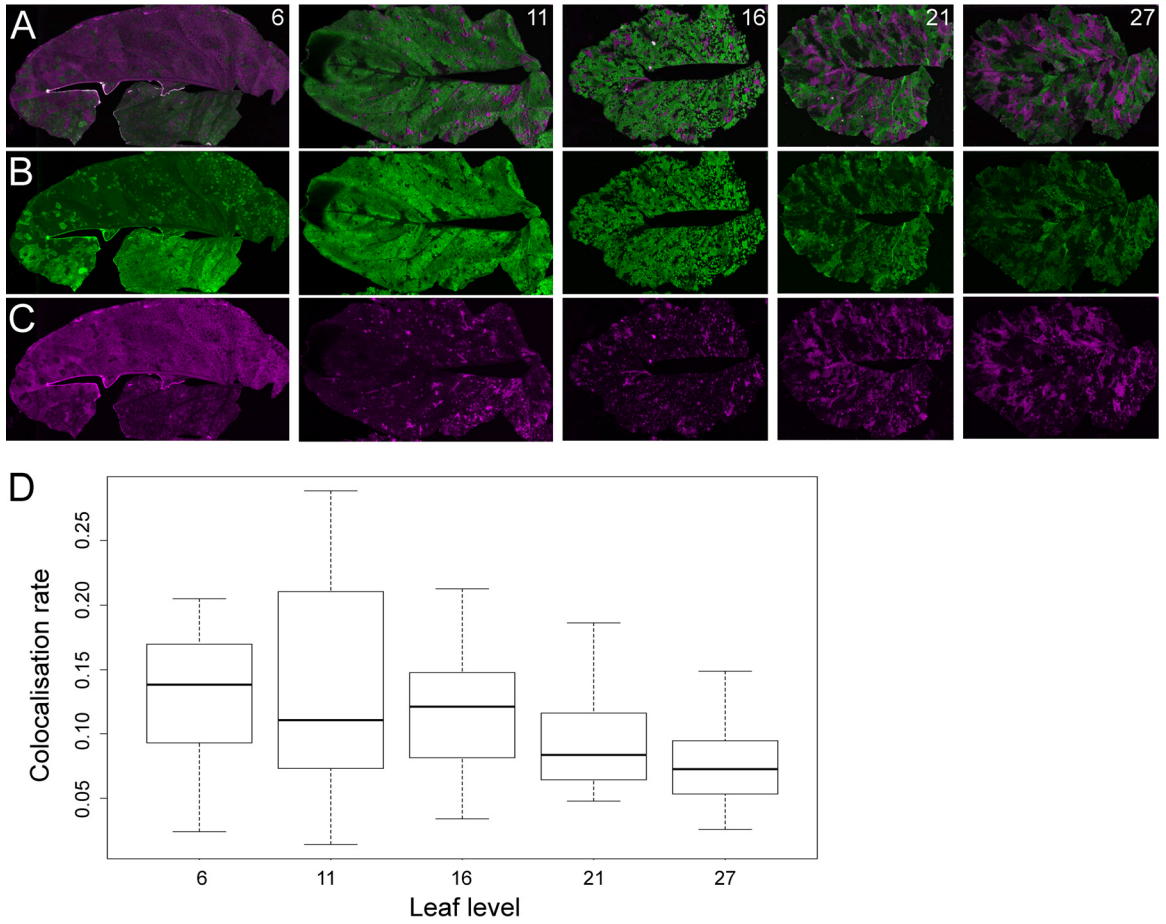

FIG 5 Analysis of spatial segregation on different leaf levels. Merged images of fluorescence in RFP and GFP channels from five leaf levels (leaf level numbers are indicated on the right corner of each image) of the same plant. (B and C) Single-channel images (GFP in green and RFP in magenta) used to create the merge images in panel A. Patches with no fluorescence could be due to the natural curvature of the leaves, to incomplete infection, or, in the last levels, to infection by mutants having lost the expression of functional fluorescence proteins. (D) Percent of the surface showing colocalization of the two types of fluorescence relative to the overall fluorescent surface in the different leaf levels.

confirming that aphids from each treatment fed on different tissues. The dynamics of the viral load in short-fed aphids and in leaf tissue (i.e., virus copies per copy of actin gene mRNA) both showed a significant peak in leaf level 27 ($P \leq 0.001$ by Tukey's honest significant difference) (compare Fig. 4B to C). This peak in viral load in leaf level 27 also was observed in long-fed aphids and in the sap (Fig. 4A). We did not observe a significant change in the copy number of the actin mRNA among leaf levels, the housekeeping transcript used to standardize viral load in leaves (not shown), suggesting that the increase in viral load late in infection (leaf level 27) was not due to a technical artifact.

To monitor spatial segregation of mRFP1 and mGFP5 clones with the passage of time and compare it in successive leaf levels, we developed a methodology that uses images of a whole leaf in the two fluorescence channels to quantitatively analyze the fluorescent landscape. Our methodology allows estimating the total leaf surface, the total fluorescent surface, and the surfaces showing either mGFP5, mRFP1, or both kinds of fluorescence (see Materials and Methods for details). A set of 20 plants was inoculated with the two fluorescent clones in a 1:1 ratio, and both fluorescent channels were scanned on five leaf levels, the same levels sampled during estimation of viral load in sap. Each level was scanned at a different time point during infection, when leaves had gone beyond the sink-to-source transition, i.e., when virus transport into the leaf level from the vasculature had stopped. Spatial segregation of the two clones was observed in all leaf levels, and we did not detect a significant change in the relative colocalization area of the two kinds of virus-derived fluorescence (linear regression; $F_{4,88} = 1.866$; $P = 0.123$) (Fig. 5A to D).

DISCUSSION

The observation of sparse primary foci showing a single type of fluorescence in systemically infected leaves (Fig. 2C) provides qualitative evidence of a very low MOI in cells colonized from the sieve elements. The collected data consistently lead to an estimated MOI of 0.072 in companion cells. That only a small fraction of the companion cells appear to be infected initially can be explained by their poor susceptibility to TuMV. An alternative explanation is that the viral load in the sap of sieve tubes (here designated viremia) is too low, with the number of virions available per susceptible companion cell being the limiting factor. The small fluctuations of viremia during systemic infection suggest that the viral load is rather stable, with variation not exceeding about 2-fold (Fig. 4). This situation contrasts with that in CaMV-infected turnip plants in which important increases of viremia after the onset of the infection probably lead to increases in the MOI (26).

Potential differences in MOI depending on the route of infection, from the sieve elements versus from other cell types, initially were suggested by the distribution of virus-derived fluorescence within the rare foci that were coinfected in systemically infected leaves. In those foci, the two fluorescent genotypes moved together from cell to cell in all directions, resulting in expanded foci homogeneously harboring the two types of fluorescence (Fig. 2D to F), and this is possible only if the MOI is high. To formally quantify this high MOI during cell-to-cell movement, we artificially generated doubly infected foci and monitored the loss of one genotype during expansion. We chose to estimate the probability of losing a genotype in one focus through the observed frequency of the doubly infected foci that presented a sector with a single kind of fluorescence. This choice is conservative, because these mixed foci might indeed stem from initial doubly infected single cells, but they also could stem from two single infections in neighbor cells. Although the latter cases are not relevant for our analysis, we cannot unambiguously distinguish them, and their inclusion in the analysis could only lead to an underestimate of the MOI.

Once the probability of losing a genotype during cell-to-cell movement was empirically established (0.165 after 14 cell-to-cell movements) (Fig. 3J), a simulation was used to infer the MOI. In this simulation, we considered a linear array of cells. Each cell was infected by the viral population of the previous cell in the row. We are aware that this is probably an oversimplified model of plant cell connections, but we used it because it has been developed previously, applied, and discussed for the estimate of the MOI of another plant virus (30), allowing a direct comparison.

Our MOI estimate during cell-to-cell movement of TuMV (MOI of ≈30 genomes/cell) is much higher than those previously reported for any other virus (for a review, see reference 45), in particular for other plant RNA viruses, such as *Tobacco mosaic virus* (TMV) (29), *Soilborne wheat mosaic virus* (SBWMV) (30), *Tobacco etch virus* (TEV) (46), and *Citrus tristeza virus* (CTV) (32). The MOI ranges between 5 and 6 for SBWMV and between 1 and 2 for TMV, TEV, and CTV. Such low MOIs are thought to be at the origin of the spatial segregation observed in plants infected by those viruses. Here, despite a larger MOI during cell-to-cell movement, a marked segregation of genotypes also was observed throughout infection, suggesting that a constant low MOI is not required for spatial segregation. Obviously, a low MOI is required at some point of the infection process to isolate genotypes, but then virus genomes can multiply enter cells when progressing into noninfected tissue and stop when encountering a previously infected one. A way to reconcile the absence of large overlap when two infection fronts collide despite the elevated MOI is to assume that viral genomes can enter cells only during a limited period of time, calculated here to be around 6 h. This observation points to a fast-acting mechanism of superinfection exclusion in TuMV-infected cells, which deserves future investigation. Although superinfection exclusion mechanisms have elegantly been shown to be a key parameter in plant virus biology, they remain largely uncharacterized (47).

This is the first evidence that the distribution of MOI values within an infected leaf is not unimodal but rather follows at least a bimodal distribution related to different MOIs in distinct subpopulations of cells. It is possible that assuming a unimodally distributed MOI among the cells of a leaf has biased MOI estimations in most previous studies with plant viruses which might have tissue tropisms similar to that of TuMV (26, 29, 46). Those studies generally have analyzed the MOI on extracted protoplasts, an approach that does not retain the spatial structure of tissues and cannot distinguish different MOIs in different cell populations. For example, we have obtained an average MOI of close to 1 in TuMV-infected leaves when estimating the MOI from extracted protoplasts (not shown). Whether the MOIs in a leaf follow a multimodal distribution in other plant viruses could be tested using a combination of *in situ* approaches, as we did in this work. Beyond plant viruses, current data on HIV also suggest a multimodal distribution of the MOIs depending on the infection route, with a low MOI when the infection takes place from cell-free virus and a high MOI during cell-to-cell virus transfers (48).

Overall, the results reported here define a detailed model of

systemic infection of leaves by TuMV. In this model, virus genotypes moving together long distances in the vasculature are individually isolated during the first phase of leaf infection. The lineages originated in primary-infected cells progress from cell to cell at a high MOI, allowing multiple infection of cells by the offspring of the initial genotype. A fast-acting superinfection exclusion mechanism restricts the subsequent mixing of these lineages to a narrow overlapping zone at the boundaries of their respective territories.

This scenario can have multiple and important consequences on the genetics and evolution of TuMV populations. For example, the maintenance of defective interfering particles in the population likely is constrained by low-MOI phases in companion cells hampering complementation and potentially resetting a clean population at leaf entry. In another example, recombination within a lineage is favored during cell-to-cell movement at high MOI, whereas recombination between different lineages is very much limited to a few cells at the frontier between foci. Remarkably, the recombinants generated in those frontier cells may have little chance to migrate to the vascular system, since all neighboring cells probably are infected and are refractory to superinfection. In other words, those recombinants likely are trapped within the cells where they are generated unless an insect vector picks them up.

More generally, it is remarkable that TuMV genotypes interact differently depending on their relatedness. At the whole-host level, each genotype interacts with others mainly through competition for leaf cells or leaf areas. In contrast, genotypes generated within a cell usually descend from the same parental genotype that created the initial infection focus in a companion cell colonized from the vasculature. Thus, beyond competition, intergenotype intracellular interactions like recombination, complementation, or cooperation are possible and likely intense during cell-to-cell movement but occur almost exclusively among kin.

The behavior of TuMV contrasts with that of CaMV, previously described in the same host (*Brassica rapa*, cv. Just Right) (26). Both viruses share many aspects of their biology, including host range, tissue specificity, vector species, and geographical distribution. We have shown previously that the MOI of CaMV varies during plant colonization and is modulated by fluctuations of the viral load in the vascular system (26). As a result, an MOI of 13 genomes per cell was estimated in leaves infected during viremia peaks, leading to 100% of the cells colonized by the two CaMV genotypes coinfecting the plant (when the two genotypes were equally frequent in leaves). This absence of spatial segregation opposes the observation reported here with TuMV in the same host. Whether CaMV genotypes can be together in primary infection sites within leaves or whether they are transiently separated and later mixed due to an absence of superinfection exclusion is unknown.

Given that differences in the colonization pattern between TuMV and CaMV have been observed in the same host plant and that the two viruses supposedly are well adapted to turnip, one can speculate on whether viruses control their colonization behavior, that is, whether the presence/absence of spatial segregation is the result of viral adaptation. Viruses could change the probability of multiple infections in primary infection sites just by adjusting the viral load in the vasculature. The logic behind this is straightforward: the more viruses uploaded in the phloem vessels, the higher the viral load and the more likely primary sites would be multiply infected. The HIV load in the vasculature and its dynamics have been shown to be determined partly by the viral genotype and are amenable to change during adaptation (49). Interestingly, we have observed that TuMV replication stopped approximately 10 days before cell death (Fig. 1A, leaf from 15 days of age and onwards), a phenomenon that can limit viral load in sap, as leaves with old infections would not contribute viruses to the sap. Alternatively, viruses could migrate as single or groups of virus particles within the vasculature, leading to the infection of primary sites by one or several genomes. The speed of superinfection exclusion is another parameter that also could be modulated to regulate the MOI. Although it is uncharacterized in plants, the mechanisms of superinfection exclusion are rather diverse in animal viruses (12–14, 18, 47), and each mechanism may take a different period of time to operate. A longer period would imply a larger time window for superinfection and the entry of more genotypes in the same cell.

ACKNOWLEDGMENTS

We are grateful to Jean-Luc Macia and Sophie Leblaye for help with plant seedlings, handling, and maintenance. We also are grateful to Gaël Thebaud for discussions on modeling approaches.

This work was funded by the grant 2010 BLAN 1704 01 form the French ANR. S.B., M.Y., and E.P. acknowledge support from the INRA SPE division, S.G. from INRA and CIRAD, and Y.M. from CNRS and IRD.

REFERENCES

1. **Carrillo FY, Sanjuan R, Moya A, Cuevas JM.** 2007. The effect of co- and superinfection on the adaptive dynamics of vesicular stomatitis virus. Infect Genet Evol **7:**69–73. http://dx.doi.org/10.1016/j.meegid.2006.04.004.
2. **Miralles R, Ferrer R, Sole RV, Moya A, Elena SF.** 2001. Multiple infection dynamics has pronounced effects on the fitness of RNA viruses. J Evol Biol **14:**654–662. http://dx.doi.org/10.1046/j.1420-9101.2001.00308.x.
3. **Nee S.** 1987. The evolution of multicompartmental genomes in viruses. J Mol Evol **25:**277–281. http://dx.doi.org/10.1007/BF02603110.
4. **Novella IS, Reissig DD, Wilke CO.** 2004. Density-dependent selection in vesicular stomatitis virus. J Virol **78:**5799–5804. http://dx.doi.org/10.1128/JVI.78.11.5799-5804.2004.
5. **Szathmary E.** 1992. Natural selection and dynamical coexistence of defective and complementing virus segments. J Theor Biol **157:**383–406. http://dx.doi.org/10.1016/S0022-5193(05)80617-4.
6. **Turner PE, Chao L.** 1998. Sex and the evolution of intrahost competition in RNA virus phi6. Genetics **150:**523–532.
7. **Turner PE, Chao L.** 1999. Prisoner's dilemma in an RNA virus. Nature **398:**441–443. http://dx.doi.org/10.1038/18913.
8. **Wilke CO, Reissig DD, Novella IS.** 2004. Replication at periodically changing multiplicity of infection promotes stable coexistence of competing viral populations. Evolution **58:**900–905. http://dx.doi.org/10.1111/j.0014-3820.2004.tb00422.x.
9. **Christen L, Seto J, Niles EG.** 1990. Superinfection exclusion of vaccinia virus in virus-infected cell cultures. Virology **174:**35–42. http://dx.doi.org/10.1016/0042-6822(90)90051-R.
10. **Huang IC, Li W, Sui J, Marasco W, Choe H, Farzan M.** 2008. Influenza A virus neuraminidase limits viral superinfection. J Virol **82:**4834–4843. http://dx.doi.org/10.1128/JVI.00079-08.
11. **Karpf AR, Lenches E, Strauss EG, Strauss JH, Brown DT.** 1997. Superinfection exclusion of alphaviruses in three mosquito cell lines persistently infected with Sindbis virus. J Virol **71:**7119–7123.
12. **Lee YM, Tscherne DM, Yun SI, Frolov I, Rice CM.** 2005. Dual mechanisms of pestiviral superinfection exclusion at entry and RNA replication. J Virol **79:**3231–3242. http://dx.doi.org/10.1128/JVI.79.6.3231-3242.2005.
13. **Lu MJ, Henning U.** 1994. Superinfection exclusion by T-even-type coliphages. Trends Microbiol **2:**137–139. http://dx.doi.org/10.1016/0966-842X(94)90601-7.
14. **Nethe M, Berkhout B, van der Kuyl AC.** 2005. Retroviral superinfection resistance. Retrovirology **2:**52. http://dx.doi.org/10.1186/1742-4690-2-52.

15. **Pepin KM, Lambeth K, Hanley KA.** 2008. Asymmetric competitive suppression between strains of dengue virus. BMC Microbiol **8:**28. http://dx.doi.org/10.1186/1471-2180-8-28.
16. **Singh IR, Suomalainen M, Varadarajan S, Garoff H, Helenius A.** 1997. Multiple mechanisms for the inhibition of entry and uncoating of superinfecting Semliki Forest virus. Virology **231:**59–71. http://dx.doi.org/10.1006/viro.1997.8492.
17. **Tscherne DM, Evans MJ, von Hahn T, Jones CT, Stamataki Z, McKeating JA, Lindenbach BD, Rice CM.** 2007. Superinfection exclusion in cells infected with hepatitis C virus. J Virol **81:**3693–3703. http://dx.doi.org/10.1128/JVI.01748-06.
18. **Whitaker-Dowling P, Youngner JS, Widnell CC, Wilcox DK.** 1983. Superinfection exclusion by vesicular stomatitis virus. Virology **131:**137–143. http://dx.doi.org/10.1016/0042-6822(83)90540-8.
19. **Dietrich C, Maiss E.** 2003. Fluorescent labelling reveals spatial separation of potyvirus populations in mixed infected Nicotiana benthamiana plants. J Gen Virol **84:**2871–2876. http://dx.doi.org/10.1099/vir.0.19245-0.
20. **Diveki Z, Salanki K, Balazs E.** 2002. Limited utility of blue fluorescent protein (BFP) in monitoring plant virus movement. Biochimie **84:**997–1002. http://dx.doi.org/10.1016/S0300-9084(02)00007-X.
21. **Giritch A, Marillonnet S, Engler C, van Eldik G, Botterman J, Klimyuk V, Gleba Y.** 2006. Rapid high-yield expression of full-size IgG antibodies in plants coinfected with noncompeting viral vectors. Proc Natl Acad Sci U S A **103:**14701–14706. http://dx.doi.org/10.1073/pnas.0606631103.
22. **Hull R, Plaskitt A.** 1970. Electron microscopy on the behavior of two strains of alfalfa mosaic virus in mixed infections. Virology **42:**773–776. http://dx.doi.org/10.1016/0042-6822(70)90322-3.
23. **Jridi C, Martin JF, Marie-Jeanne V, Labonne G, Blanc S.** 2006. Distinct viral populations differentiate and evolve independently in a single perennial host plant. J Virol **80:**2349–2357. http://dx.doi.org/10.1128/JVI.80.5.2349-2357.2006.
24. **Takahashi T, Sugawara T, Yamatsuta T, Isogai M, Natsuaki T, Yoshikawa N.** 2007. Analysis of the spatial distribution of identical and two distinct virus populations differently labeled with cyan and yellow fluorescent proteins in coinfected plants. Phytopathology **97:**1200–1206. http://dx.doi.org/10.1094/PHYTO-97-10-1200.
25. **Takeshita M, Shigemune N, Kikuhara K, Furuya N, Takanami Y.** 2004. Spatial analysis for exclusive interactions between subgroups I and II of cucumber mosaic virus in cowpea. Virology **328:**45–51. http://dx.doi.org/10.1016/j.virol.2004.06.046.
26. **Gutiérrez S, Yvon M, Thébaud G, Monsion B, Michalakis Y, Blanc S.** 2010. Dynamics of the multiplicity of cellular infection in a plant virus. PLoS Pathog **6:**e1001113. http://dx.doi.org/10.1371/journal.ppat.1001113.
27. **Bull JC, Godfray HC, O'Reilly DR.** 2001. Persistence of an occlusion-negative recombinant nucleopolyhedrovirus in Trichoplusia ni indicates high multiplicity of cellular infection. Appl Environ Microbiol **67:**5204–5209. http://dx.doi.org/10.1128/AEM.67.11.5204-5209.2001.
28. **Gutierrez S, Thebaud G, Smith DR, Kenney JL, Weaver SC.** 2015. Demographics of natural oral infection of mosquitos by Venezuelan equine encephalitis virus. J Virol **89:**4020–4022. http://dx.doi.org/10.1128/JVI.03265-14.
29. **Gonzalez-Jara P, Fraile A, Canto T, Garcia-Arenal F.** 2009. The multiplicity of infection of a plant virus varies during colonization of its eukaryotic host. J Virol **83:**7487–7494. http://dx.doi.org/10.1128/JVI.00636-09.
30. **Miyashita S, Kishino H.** 2010. Estimation of the size of genetic bottlenecks in cell-to-cell movement of soil-borne wheat mosaic virus and the possible role of the bottlenecks in speeding up selection of variations in trans-acting genes or elements. J Virol **84:**1828–1837. http://dx.doi.org/10.1128/JVI.01890-09.
31. **Tromas N, Elena SF.** 2010. The rate and spectrum of spontaneous mutations in a plant RNA virus. Genetics **185:**983–989. http://dx.doi.org/10.1534/genetics.110.115915.
32. **Bergua M, Zwart MP, El-Mohtar C, Shilts T, Elena SF, Folimonova SY.** 2014. A viral protein mediates superinfection exclusion at the whole-organism level but is not required for exclusion at the cellular level. J Virol **88:**11327–11338. http://dx.doi.org/10.1128/JVI.01612-14.
33. **Josefsson L, King MS, Makitalo B, Brannstrom J, Shao W, Maldarelli F, Kearney MF, Hu WS, Chen J, Gaines H, Mellors JW, Albert J, Coffin JM, Palmer SE.** 2011. Majority of CD4+ T cells from peripheral blood of HIV-1-infected individuals contain only one HIV DNA molecule. Proc Natl Acad Sci U S A **108:**11199–11204. http://dx.doi.org/10.1073/pnas.1107729108.
34. **Jung A, Maier R, Vartanian JP, Bocharov G, Jung V, Fischer U, Meese E, Wain-Hobson S, Meyerhans A.** 2002. Multiply infected spleen cells in HIV patients. Nature **418:**144. http://dx.doi.org/10.1038/418144a.
35. **Josefsson L, Palmer S, Faria NR, Lemey P, Casazza J, Ambrozak D, Kearney M, Shao W, Kottilil S, Sneller M, Mellors J, Coffin JM, Maldarelli F.** 2013. Single cell analysis of lymph node tissue from HIV-1 infected patients reveals that the majority of CD4+ T-cells contain one HIV-1 DNA molecule. PLoS Pathog **9:**e1003432. http://dx.doi.org/10.1371/journal.ppat.1003432.
36. **Kalderon D, Roberts BL, Richardson WD, Smith AE.** 1984. A short amino acid sequence able to specify nuclear location. Cell **39:**499–509. http://dx.doi.org/10.1016/0092-8674(84)90457-4.
37. **Beauchemin C, Bougie V, Laliberte JF.** 2005. Simultaneous production of two foreign proteins from a polyvirus-based vector. Virus Res **112:**1–8. http://dx.doi.org/10.1016/j.virusres.2005.03.001.
38. **Murphy JF, Rhoads RE, Hunt AG, Shaw JG.** 1990. The VPg of tobacco etch virus RNA is the 49-kDa proteinase or the N-terminal 24-kDa part of the proteinase. Virology **178:**285–288. http://dx.doi.org/10.1016/0042-6822(90)90405-G.
39. **Sako N.** 1980. Loss of aphid transmissibility of turnip mosaic virus. Phytopathology **70:**647–649. http://dx.doi.org/10.1094/Phyto-70-647.
40. **Cotton S, Grangeon R, Thivierge K, Mathieu I, Ide C, Wei T, Wang A, Laliberte JF.** 2009. Turnip mosaic virus RNA replication complex vesicles are mobile, align with microfilaments, and are each derived from a single viral genome. J Virol **83:**10460–10471. http://dx.doi.org/10.1128/JVI.00819-09.
41. **Ruijter JM, Ramakers C, Hoogaars WM, Karlen Y, Bakker O, van den Hoff MJ, Moorman AF.** 2009. Amplification efficiency: linking baseline and bias in the analysis of quantitative PCR data. Nucleic Acids Res **37:**e45. http://dx.doi.org/10.1093/nar/gkp045.
42. **Schneider CA, Rasband WS, Eliceiri KW.** 2012. NIH Image to ImageJ: 25 years of image analysis. Nat Methods **9:**671–675. http://dx.doi.org/10.1038/nmeth.2089.
43. **Gutiérrez S, Yvon M, Pirolles E, Garzo E, Fereres A, Michalakis Y, Blanc S.** 2012. Circulating virus load determines the size of bottlenecks in viral populations progressing within a host. PLoS Pathog **8:**e1003009. http://dx.doi.org/10.1371/journal.ppat.1003009.
44. **Cleveland WS.** 1981. LOWESS: a program for smoothing scatterplots by robust locally weighted regression. Am Stat **35:**54.
45. **Gutiérrez S, Michalakis Y, Blanc S.** 2012. Virus population bottlenecks during within-host progression and host-to-host transmission. Curr Opin Virol **2:**546–555. http://dx.doi.org/10.1016/j.coviro.2012.08.001.
46. **Tromas N, Zwart MP, Lafforgue G, Elena SF.** 2014. Within-host spatiotemporal dynamics of plant virus infection at the cellular level. PLoS Genet **10:**e1004186. http://dx.doi.org/10.1371/journal.pgen.1004186.
47. **Folimonova SY.** 2012. Superinfection exclusion is an active virus-controlled function that requires a specific viral protein. J Virol **86:**5554–5561. http://dx.doi.org/10.1128/JVI.00310-12.
48. **Duncan CJ, Williams JP, Schiffner T, Gartner K, Ochsenbauer C, Kappes J, Russell RA, Frater J, Sattentau QJ.** 2014. High-multiplicity HIV-1 infection and neutralizing antibody evasion mediated by the macrophage-T cell virological synapse. J Virol **88:**2025–2034. http://dx.doi.org/10.1128/JVI.03245-13.
49. **Alizon S, von Wyl V, Stadler T, Kouyos RD, Yerly S, Hirschel B, Boni J, Shah C, Klimkait T, Furrer H, Rauch A, Vernazza PL, Bernasconi E, Battegay M, Burgisser P, Telenti A, Gunthard HF, Bonhoeffer S, Swiss HIV Cohort Study.** 2010. Phylogenetic approach reveals that virus genotype largely determines HIV set-point viral load. PLoS Pathog **6:**e1001123. http://dx.doi.org/10.1371/journal.ppat.1001123.